Physical and Chemical Analyses on Single-Source Precursor-Grown CdS Semiconductor Nanomaterials

Mathieu Fregnaux,[†,‡] Didier Arl,[†,‡] Stéphane Dalmasso,*[,‡] Jean-Jacques Gaumet,[†] and Jean-Pierre Laurenti[‡]

Laboratoire de Spectrométrie de Masse et de Chimie Lase and Laboratoire de Physique des Milieux Denses, Institut Jean Barriol, Université Paul Verlaine-Metz, 1 Boulevard Arago, F-57078 Metz Cedex 03, France

Received: May 10, 2010; Revised Manuscript Received: September 9, 2010

CdS quantum dots (QDs) are synthesized by the single-source precursor thermal method. Use of a temperature ramp allows faster elaboration of high-quality smaller nanoparticles in size. A cross-disciplinary study between chemical analyses and physical techniques provides consistent data for these small size QDs. Joint X-ray diffraction, mass spectrometry, transmission electron microscopy, and optical spectrometry techniques give a consistent picture about the crystalline structure, average size, and size dispersion of the QDs as well as their optical spectral response in correlation with their size via quantum confinement effects. These QDs have great potential as light-emitting devices because of their tunable response wavelength in the near UV and blue part of the visible spectrum range.

1. Introduction

The development of nanotechnologies implies fundamental and applied research on nanosemiconductors (nano-SCs). New technologies and applications for these nanoscale particles have been reported in the past decade due to improvements in the chemical synthetic methods. These materials can have many applications including biomarkers,[1−3] solar cells,[4−6] and lighting technologies.[7] In this context, II−VI nano-SCs are very interesting systems due to the evolution of their electronic properties during the growth process, e.g., in cadmium sulfide (CdS) the fundamental excitonic transition evolutes from 4.78 (diameter 1.28 nm) to 2.60 eV (diameter 9.60 nm) due to quantum confinement effects.[8−11] The same behavior is observed on other II−VI quantum dots (QDs), particularly in the visible wavelength range for cadmium selenide (CdSe).[9−12]

A nanoparticle consists of an aggregate of $\sim 10-10^5$ atoms bonded together in a radius ranging between ~1 and 100 nm. Therefore, different approaches for the elaboration of nano-SC have been developed such as chemical synthesis, self-assembling methods, electrochemical methods, chemical vapor deposition, hydride vapor phase epitaxy, metal−organic vapor phase epitaxy, or molecular beam epitaxy. However, a cost-effective way to produce this kind of cluster has been demonstrated by the solid-state method.[8,9,13] In that case, semiconducting nanocomposite materials have been mostly prepared by inclusion of preformed particles in different types of matrix or by polymerization of precursors in hydrolytic or nonhydrolytic ways. The sol−gel technique provides the production of inorganic or mixed organic−inorganic compounds at low reaction temperature;[14−16] due to the fact that the reactant mixture is realized at the molecular scale, the temperature of the reaction is indeed clearly lowered. This ensures an accurate adjustment of the properties of the synthesized clusters.[17] The single-source precursor methodology, used in our work, is based on introduction of a chalcogenide cadmium precursor in an alkylamine solvent to produce cadmium thiophenolates.[18] The elaboration of QDs consists of two separate steps, i.e., (i) synthesis of thiophenolate precursors based on the sol−gel process of an organic−inorganic mixture of reactants followed by (ii) thermal growth by stages of nanoclusters by denaturating the precursor structure in an alkylamine solvent at different temperatures. As previously reported, thermal growth consists of applying a ramp of temperature, which enables us to get QDs with smaller sizes.[12]

In this work, we report a physics/chemistry cross-disciplinary study of single-source precursor-grown CdS QDs. Chemical analysis is performed by mass spectrometry (MS), which provides background data about the composition, size, surface, and stability of nanoparticles.[19] Additional data about the crystalline structure and size distribution of the QDs are obtained from X-ray diffraction (XRD) and transmission electron microscopy (TEM). Physical investigation uses optical spectrometry of nanodispersions, photoluminescence (PL) and absorption, which allows analysis of quantum size effects. The confinement of electron−hole pairs in small size crystals significantly enhances transition efficiencies and enables us to operate at room temperature (RT).

2. Elaboration of CdS QDs by Thermal Growth

CdS QDs were prepared by a thermal growing process of cadmium thiophenolate $Cd_{10}S_4$ ($\equiv [(CH_3)_4N]_4[S_4Cd_{10}(SPh)_{16}]$) mixed in hexadecylamine [HDA, melting point = 47 °C]. This precursor was prepared by literature methods and confirmed by ESI-TOF MS[20,21] (see section 4.1.1). The alkylamine HDA was used as a solvent and as a functionalizing reactant. The chemicals were put in a three-neck round-bottom flask under an argon atmosphere. The system was then heated in an oil bath. Figure 1 shows schematically the thermal extraction profile used in our work.

The process which was first developed to synthesize CdSe QDs[12] was extended to CdS QDs. It combines an increase of the temperature with aging time for having homogeneized QDs.

* To whom correspondence should be addressed. Phone: (33) 3 87 31 58 45. Fax: (33) 3 87 31 58 01. E-mail: dalmasso@univ-metz.fr.
† Laboratoire de Spectrométrie de Masse et de Chimie Laser.
‡ Laboratoire de Physique des Milieux Denses.

10.1021/jp104233x
Published on Web 09/24/2010

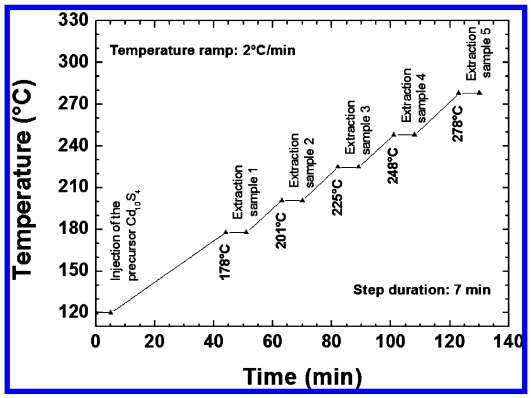

Figure 1. Extraction profile by stages of the thermal growth of QDs in an alkylamine solvent (HDA). After initial injection of the precursor $Cd_{10}S_4$ at 120 °C, each extraction step had a 7 min duration before sampling ~100 mg of product and applying the next increase in temperature.

Briefly, it consists of (i) applying a climbing temperature scale from 120 (injection of the precursor $Cd_{10}S_4$) to 278 °C at a heating rate of 2 °C/min, (ii) establishing 7 min steps in order to avoid reaction inertia effects, and (iii) extracting some QD solution at the end of every step. The duration time for the temperature steps results from balancing the required time for stabilization with the relatively slow kinetics of precursor denaturation by a thiophenolate−amine exchange. Compared with other thermal growth techniques,[11] this ensures production of QDs with smaller diameters at lower temperatures. Besides, shorter reaction times are required, i.e., the first sample is obtained at 178 °C after 50 min of reaction, and the duration of the whole process does not exceed 130 min.

After extraction of an aliquot out of the reaction bath and its quasi-instantaneous solidification, the CdS QDs are kept in the dark at RT. The organic alkyl crown-capping ligand was thick enough to preserve the CdS nano-SCs. For characterization purposes, CdS QDs are washed three times with methanol (MeOH, 98%) to eliminate the organic ligands.

3. Experimental Techniques for Characterization of QDs

3.1. Mass Spectrometry. Both precursors and nanomaterials were characterized by MS using two different soft ionization techniques: electrospray source ionization (ESI) and matrix-assisted laser desorption ionization (MALDI). These two techniques are especially useful in producing molecular or pseudomolecular ions from large molecular systems (polymers, peptides, biomolecules, ...) because they overcome the propensity of these molecules to fragment when severely ionized.

3.1.1. Analyses on Precursors. Mass spectra on precursors were performed in negative-ion mode using ESI coupled to a quadrupole time-of-flight mass spectrometer (microTOF-Q 98, Bruker Daltonics, Service Commun de Spectrométrie de Masse et de Chromatographie, Université Henri Poincaré, Nancy I). The soft ionization process was induced by a spray voltage ranging from −500 to −3000 V.

3.1.2. Analyses on Nanomaterials. MS analyses on thermally grown QDs were carried out on a MALDI coupled to a time of flight (MALDI-TOF MS) instrument (Reflex IV, Bruker, Nd:YAG laser, wavelength 266 nm, maximum output energy = 1.5 mJ per pulse) with dithranol used as the matrix. CdS−HDA QDs were dispersed in dry chloroform, mixed with solutions of the matrix, and spotted onto a target plate before irradiation. Mass spectra were measured with the laser between 30% and 50% full power. Every sample was characterized by at least six mass spectra to average the measures.

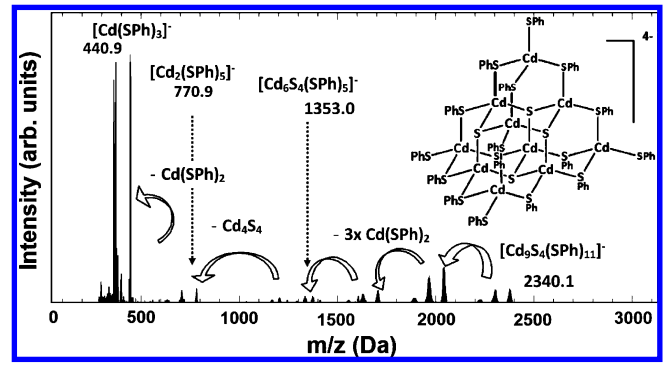

Figure 2. ESI-QTOF mass spectrum of $[Cd_{10}S_4(SPh)_{16}]^{4-}$.

3.2. X-ray Powder Diffraction. A Bruker AXS D8 diffractometer operating with a Cu anode ($K\alpha_1$ 0.15405 nm) was used for X-ray powder diffraction spectra. For ensuring organic ligand removal, QDs were washed in methanol. After solvent evaporation, CdS QD powders were dropped on silicon (100) wafers to perform slow $\theta/2\theta$ acquisition scans. Six to eight hours were necessary to optimize the signal-to-noise ratio.

3.3. Transmission Electron Microscopy. TEM was performed on a FEI CM 200 microscope operating at 200 kV and equipped with a Gatan CCD camera for digital micrograph acquisition. High-magnification (~500 000×) bright field images were analyzed using image processing software, in a semiautomatic mode, to get QD sizes. For each analyzed sample, the average size and size distribution were obtained from 100 single particles.

This procedure allows statistical analysis of all types of divided materials by dispersion of isolated particles onto a film on a support grid.[22] A homogeneous suspension of a divided material (fiber, polymer, virus, nanomaterial, ...) is obtained by addition of a volatile solvent to the solid, in order to produce a relatively less concentrated solution. The suspension is stirred to separate the residual aggregates of particles.

QDs of CdS−HDA were placed in toluene and sonicated for 5 min. A drop of the solution was placed on a 200 mesh Cu grid coated with thin amorphous carbon film and left for 15 min for solvent evaporation.

3.4. Optical Spectrometry. The QDs were diluted in toluene (1 mg of CdS−HDA in 1 mL of toluene). For absorption measurements, a white light produced by a Quartz-Iode source illuminated the bath. The transmitted light was dispersed by grating and analyzed by a CCD camera with a resolution of 0.23 nm. For PL spectroscopy a He−Cd laser (wavelength 325 nm, photon energy 3.82 eV) excited the same bath of QDs. The emitted signal was dispersed and analyzed by a similar spectrometric setup. All measurements were performed at RT.

4. Results

4.1. Mass Spectrometry. ***4.1.1. ESI TOF-Q MS Analysis on $[Cd_{10}S_4(SPh)_{16}](CH_3)_4N]_4$ Precursor.*** Electrospray coupled with time-of-flight mass spectrometry allows rapid analysis of metal thiophenolate precursors. This is the strength of mass spectrometry, to show a specific fingerprint for the precursors. Mass spectra for positive- and negative-ion mode have been published elsewhere.[19,20]

In the present case, ESI mass spectrometry was performed for each cadmium thiophenolate sample for quality and stability control. In Figure 2, in the negative mode, a pseudomolecular ion at m/z 2340 is detected corresponding to the singly charged species $[Cd_9S_4(SPh)_{11}]^-$ directly connected to the $Cd_{10}S_4$ precur-

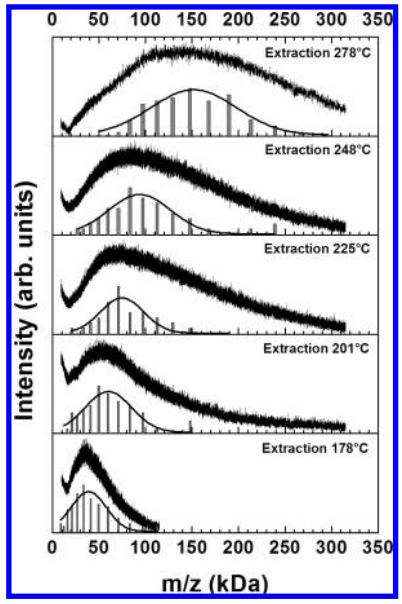

Figure 3. MALDI-TOF mass spectra (full lines) of thermally grown QDs of CdS−HDA using dithranol as matrix. The mass distributions were deduced from the size distributions obtained by TEM image analysis (section 4.3). A close comparison is detailed in section 5.

sor via the loss of 3 neutral fragments $(CH_3)_4N(SPh)$, 1 neutral fragment $Cd(SPh)_2$, and the $(CH_3)_4N^+$ counterion.

Moreover, this specific fingerprint of $Cd_{10}S_4$ shows the regular loss of $Cd(SPh)_2$ from the precursor capping that surrounds a Cd_4S_4 core previously detected in tandem mass spectrometry.[23] This explains a mass difference of 578 between the highest specific core-related species $Cd_6S_4(SPh)_5^-$ at *m/z* 1353 and a capping-related species $Cd_2(SPh)_5^-$ at *m/z* 771, which corresponds to the Cd_4S_4 core. This result may give some information on the processes involved in the cadmium thiophenolates thermal activation to generate CdS QDs. From MS data, the growing process could be described as an association of Cd_4S_4 moieties which will go to CdS QDs via successive removal of $Cd(SPh)_2$ fragments as already described by Cumberland et al.[11] This "polymer" approach is still under investigation in our groups.

4.1.2. MALDI-TOF MS Analysis on CdS−HDA Clusters. The MALDI-TOF MS technique allows us to estimate the size of QDs. Figure 3 shows MALDI-TOF mass spectra (full lines) for the CdS−HDA QDs extracted at different temperatures. The average mass numbers *m/z* detected for the five samples extracted during the thermal growth process (Figure 1) are listed in Table 1. They shift from *m/z* 36 000 (178 °C) to 134 000 (278 °C). All signals have a wide Gaussian profile which is broadened when temperature increases. This broadening could be linked to a fragmentation process for larger particles and also to the isotopic ratio (eight isotope peaks for each cadmium atom). Indeed, such clusters are composed of a high number of CdS units (from 200 for 178 °C to 900 units for 278 °C) which makes them very sensitive to collisions or perturbations and can explain their tendency to easily lose fragments. The laser power was selected to (i) optimize the high molecular weight peak and (ii) avoid fragmentation of QDs due to the intense photonic energy required to obtain a signal. The resolution available from the linear mode in MALDI-TOF MS allows to measure the peak full width at half-maximum (fwhm) and therefore to assess the size dispersion. Thus, MALDI-TOF mass spectra enable us to estimate the number of CdS units in the QD and therefore to evaluate the size and size dispersity of the QDs.

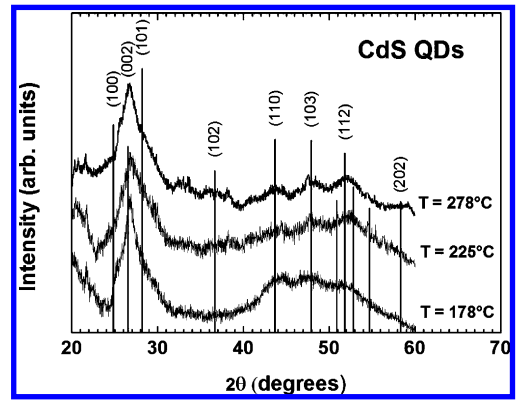

Figure 4. X-ray powder diffractograms of the CdS QDs extracted at temperatures of 178, 225, and 278 °C. The vertical lines indicate the standard hexagonal CdS bulk peak positions from Pearson's Crystal Data: CdS 1120352.

As previously reported by Khitrov et al.,[24] QD size can be deduced from their quantity of pattern by using the model of Inoue.[25] Assuming that the QDs exhibit a spherical morphology, the diameter *d* of the QDs is deduced from

$$d^3 = \frac{6V_m(CdS)_n}{\pi N_a} \quad (1)$$

where $(CdS)_n$ is the number of repeating CdS units in the QD deduced from the mass spectra, N_a is Avogadro's number, and V_m is the molar volume of bulk CdS. Taking $V_m = 3.03 \times 10^{22}$ nm^3/mol,[26] this gives the diameters of the QDs reported in Table 1.

In QD size study, mass spectra were fitted with a Gaussian profile to determine the size distribution of the clusters. This approach has the tendency to overestimate the size dispersity. Indeed, the isotopic ratio and fragmentation processes are not taken into consideration in this model. As mentioned above, they may be in part responsible of the peak broadening on the mass spectra. However, in spite of this overestimated size distribution, these results are consistent with those obtained by TEM analysis (section 4.3).

4.2. X-ray Powder Diffraction. Figure 4 shows the X-ray powder diffraction pattern of samples extracted at 178, 225, and 278 °C, respectively. Due to the small size of the QDs, the

TABLE 1: Summary of the MALDI-TOF MS Results for the Five Samples Extracted during the Thermal Growth Process[a]

extraction temperature (°C)	MALDI-TOF MS peak (Da)	MALDI-TOF MS fwhm peak (Da)	average diameter (nm)	size dispersity (%)
178	36 000	38 000	2.9 ± 0.5	17
201	55 000	61 000	3.3 ± 0.6	18
225	72 000	86 000	3.6 ± 0.7	19
248	101 000	120 000	4.0 ± 0.8	20
278	134 000	173 000	4.5 ± 1.0	22

[a] Data about the average diameter and size dispersity of the corresponding QDs are deduced from the MS technique.

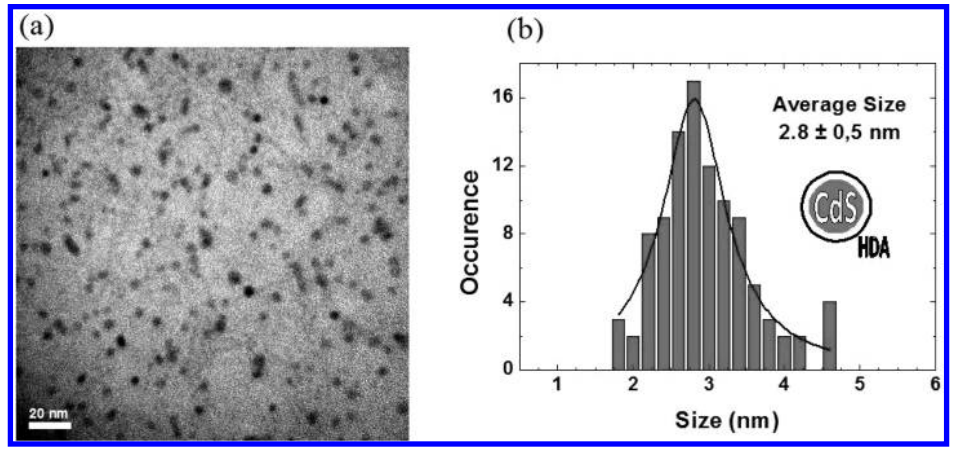

Figure 5. Bright field TEM image of CdS QDs functionalized with HDA extracted at 178 °C ((a) scale bar length is 20 nm) and its corresponding size distribution fitted by a Gaussian profile (b).

TABLE 2: Summary of Data Collected by Various Techniques for the Different Synthesized CdS-HDA QDs: Diameters and Size Distributions after MALDI-TOF MS and TEM and Fundamental Absorption Wavelengths and Energies

	MALDI-TOF MS		TEM measurements		fundamental absorption	
extraction temperature (°C)	diameter (nm)	dispersity (%)	diameter (nm)	dispersity (%)	wavelength (nm)	energy (eV)
178	2.9 ± 0.5	17	2.8 ± 0.5	18	371.0	3.35
201	3.3 ± 0.6	18	3.3 ± 0.55	17	388.5	3.19
225	3.6 ± 0.7	19	3.6 ± 0.5	14	403.2	3.08
248	4.0 ± 0.8	20	3.9 ± 0.5	13	407.7	3.04
278	4.5 ± 1.0	22	4.5 ± 0.5	11	413.0	3.01

diffractograms exhibit broad diffraction peaks from which identification of the crystalline structure is nevertheless possible. The diffraction patterns for all three samples are consistent with the hexagonal structure for CdS bulk (vertical bars). Even the smallest QDs are clearly hexagonal (würtzite phase), in contrast with previous results on CdS nano-SCs, which indicated a cubic phase for such clusters obtained with a similar synthetic route[27] or via size-selective precipitation.[8] However, the diffractograms do not allow determination of an average size of the QDs.

4.3. Transmission Electron Microscopy. A typical TEM image is shown in Figure 5a for the CdS−HDA QDs extracted at 178 °C. Analysis of the data leads to the size distribution (Figure 5) with an average diameter of 2.8 ± 0.5 nm.

Data collected by TEM measurements and optical absorption (section 4.4) are summarized in Table 2 and compared with the MALDI-TOF MS results. QD diameters which have been deduced from MALDI-TOF MS analyses are consistent with the TEM analyses. A close comparison of mass distributions obtained by MALDI-TOF MS and extrapolated from TEM analysis for all the samples will be detailed in section 5.

In Table 2, all samples exhibit a size dispersity higher than those reported in the previous study on CdSe with the same thermal growth process.[12] Indeed, this work involved CdSe QDs ranging from 2.2 to 3.3 nm average diameter with a size dispersion ranging between 8% and 19%. Likewise, some previous studies[11,24] have a smaller size dispersity ranging from 5% to 13%. However, in these studies stating a reduced size dispersity, another protocol of elaboration was used, i.e., extraction of QDs at a fixed temperature in relation to time. Moreover, these differences in size dispersity can be explained by an additional step in their protocol. Before extracting the QDs, the reaction mixture was cooled down by 20 °C and then left overnight for QDs annealing. The absence of an annealing process in our work may be responsible for the significant size dispersity that we observed. Some changes in our protocol are in progress in order to improve this point. From a MS point of view, the main contribution of cadmium isotopes will be discussed in section 5.

4.4. Optical Spectrometry. Figure 6 shows the RT absorption (a) and PL (b) spectra obtained from the different CdS QDs diluted in a toluene bath as described above. The general features compare with previous results in the field of high-quality QDs.[9,11]

In particular, (i) the fundamental excitonic transition ($n = 1$) merges from the absorption spectra (Figure 7a) as a band characteristic of quantum confinement. Gaussian fit allows us to extract the energies of these fundamental transitions in the energy range 3.01−3.35 eV (Table 2), i.e., well beyond the optical band gap of bulk CdS at 2.42 eV; however, probably

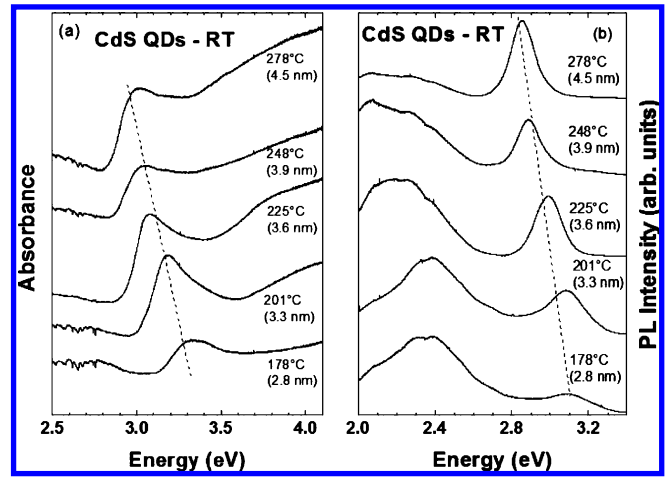

Figure 6. RT absorption (a) and PL (b) spectra of CdS QDs diluted in toluene after extraction at various temperatures indicated near every spectrum. The average diameters of the QDs, obtained from TEM measurements, are displayed within parentheses. The energy shift associated with carrier quantum confinement is emphasized by dashed guidelines.

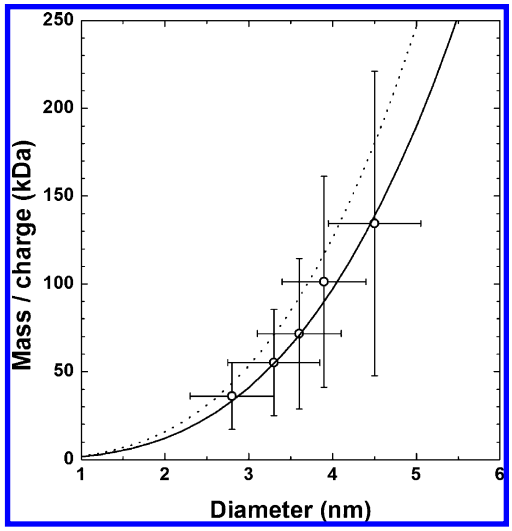

Figure 7. Mass/charge of the CdS−HDA QDs corresponding to the peaks in the MALDI TOF spectra as a function of the average diameter deduced from TEM image analysis (open circles); error bars display the fwhm of the Gaussian profiles fitting the series of data. Full and dashed lines are obtained from eq 1 assuming, respectively, spherical and prolate (1.3 correcting factor) QD morphologies.

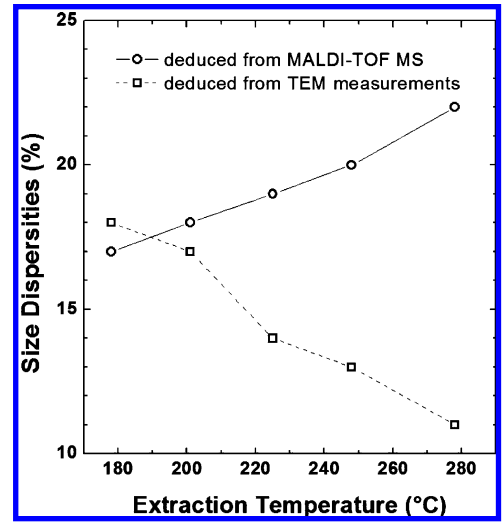

Figure 8. Comparison of size dispersities deduced from MALDI-TOF MS (open circles) and TEM analyses (open squares) as a function of extraction temperatures of QDs. The full and dashed lines are guidelines for the eyes.

due to size dispersion, the transitions involving higher confinement levels ($n > 1$) are not resolved. (ii) The PL spectra (Figure 6b) exhibit a significant recombination band close to the fundamental absorption edge, which indicates the excitonic character of the observed transition. (iii) In both spectra series, the quantum size effect is evidenced by a downshift of the transition energies when the extraction temperature increases; the blue shift effect is consistent with the average diameter of QDs determined from MS and TEM measurements.

Besides the near band edge emission, a broad low-energy band located in the energy range 2.2−2.4 eV is observed, as already reported previously.[28−30] Lying ~0.7 eV below the near band edge one, this emission has been attributed to surface states associated to S vacancies.[29,31−33] Our PL spectra exhibit a change of relative intensities between the two bands: when the QD size increases (extraction temperature increase), the magnitude of the low-energy band decreases in favor of that of the band edge one. This behavior would agree with the surface origin of the low-energy band, since surface effects affect most significantly the physical properties of the smallest size nanoparticles.[33] More detailed studies in this field will be performed and reported elsewhere.

5. Discussion and Conclusions

As already mentioned above, the QDs diameters obtained from MALDI-TOF MS analyses and TEM measurements are consistent (see Table 2). This is illustrated in Figure 7, where MALDI-TOF MS data are plotted vs TEM ones (open circles). For comparison, the mass/diameter correspondence is drawn by eq 1 assuming a spherical (full line) and prolate (dashed line) morphology of the QDs. In contrast with previous data on ZnS QDs,[24] the agreement of our data with the Inoue model[25] is verified assuming a singly charged QD species. Both morphologies fit the experimental data inside the fwhm of the Gaussian profiles illustrated by error bars.

MALDI-TOF MS and TEM analyses revealed significant size dispersion which could be correlated to the nonresolution of $n > 1$ transitions in absorption spectra. To compare closely the dispersions revealed by these two techniques, we plotted on the mass spectra of Figure 3 the mass distributions extrapolated by using eq 1 from the size distributions obtained by TEM image analysis. The overall agreement between both series of data is clearly illustrated.

Nevertheless, the respective size dispersities deduced from MALDI-TOF mass spectra and TEM measurements are compared in Figure 8. Note that beyond a QD size corresponding to an extraction temperature ≈ 200 °C, the two data series tend to separate. The size dispersity deduced from MALDI-TOF increases with the extraction temperature (QD size increase). This seems to indicate a QD growth mechanism via Ostwald ripening. On the other hand, the size dispersity deduced from TEM decreases during the growth process. Concerning size dispersion, the growth condition of our QDs, under limited monomer,[34] can be described in two steps: (i) the size distribution narrows during the first few minutes (so called focusing step) and (ii) then starts to broaden (so called defocusing or Ostwald ripening step). In our case, the protocol with the ramp temperature would be so fast that we would not reach the defocusing step, explaining the continuous decrease of the size dispersity observed by TEM analysis. Thus, the increasing size dispersity observed in MS would not result from QD growth under Ostwald ripening but could rather be attributed to the analysis method. Indeed, MALDI-TOF MS involves fragmentation processes. Also, the QDs are composed of a high number of atoms which makes them very sensitive to collisions or perturbations. Finally, the isotopic ratio of cadmium atoms can lead to mass spectra broadening. These factors could explain the mass spectra broadening observed for QDs with a diameter higher than 3.3 nm. Consequently, MS may have the tendency to overestimate the size dispersity of the largest particles.

Figure 9 shows a plot of the average diameters determined by MALDI-TOF MS and TEM measurements vs the corresponding fundamental transition energies extracted from the absorption spectra, together with a commonly admitted empirical sizing curve.[35] The equation of this sizing curve was established by the authors of ref 35 from experimental data from the literature. These size data were all originally determined by TEM measurements, except those of the smallest CdS QDs which were extracted from XRD.

Considering (i) the size dispersion (displayed by error bars) and (ii) the scattering of the numerous data fitted by the sizing curve, our results are consistent with this empirical energy−size correspondence.

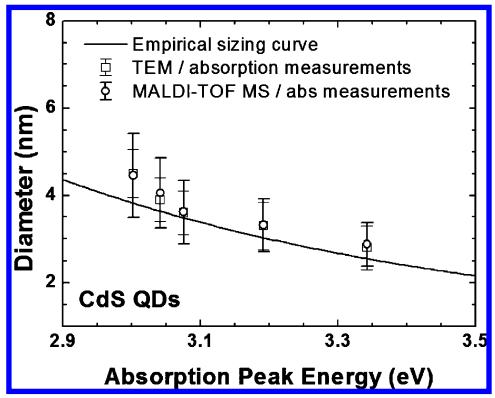

Figure 9. Average diameters of CdS QDs after TEM (open squares) and MALDI-TOF MS (open circles) measurements vs the corresponding fundamental absorption energies, compared with the size−energy empirical correspondence (Figure 2 of ref 31). Error bars illustrate the size dispersion from measurements.

The size dispersion evidenced by these joint characterization techniques should be correlated with the elaboration protocol used in this work, i.e., applying a temperature ramp for thermal growth of precursors with regular sampling of various sizes QDs without the annealing process. However, this protocol offers significant advantages: obtaining (i) QDs as small as ∼2.8 nm in diameter and (ii) a complete set of QDs with diameters ranging from ∼2.8 to ∼4.5 nm during a growth process which does not exceed 130 min in duration. Even for the smallest QDs, the particles crystallized in hexagonal structure (würtzite phase). Therefore, optimization of the protocol to reduce the size dispersion is a worthwhile task which is now in progress.

In conclusion, joint MS, XRD, TEM, and optical spectrometry techniques provide a consistent picture about the crystalline structure, average size, and size dispersion of single-source precursor-grown CdS QDs as well as their optical spectral response in correlation with their size via quantum confinement effects. Optimizations of the original elaboration protocol tested here are in progress in order to improve the size selectivity. The samples obtained will be closely checked by near band edge optical spectrometry. Besides, investigations on surface defects will be performed by a systematic study of the low-energy PL band in close relation with elaboration parameters.

Acknowledgment. The authors would like to thank Pr. G. Kirsch for his help in the synthesis of all nanomaterials and their precursors. They also wish to thank Dr. Y. Zhang for performing TEM images, Dr. S. Diliberto for his help in XRD measurements, and P. Franchetti for technical assistance. M.F. acknowledges the Ministère de l'Enseignement Supérieur et de la Recherche (France) for grants.

References and Notes

(1) Larson, D. R.; Zipfel, W. R.; Williams, R. M.; Clark, S. W.; Bruchez, M. P.; Wise, F. W.; Webb, W. W. *Science* **2003**, *300*, 1434–1436.

(2) Gao, X.; Chan, W. C. W.; Nie, S. *J. Biomed. Opt.* **2002**, *7*, 532–537.

(3) Shen, R.; Shen, X.; Zhang, Z.; Li, Y.; Liu, S.; Liu, H. *J. Am. Chem. Soc.* **2010**, *132*, 8627–8634.

(4) Nozik, A. J. *Physica E* **2002**, *14*, 115–120.

(5) Huynh, W. U.; Dittmer, J. J.; Libby, W. C.; Whiting, G. L.; Alivisatos, A. P. *Adv. Funct. Mater.* **2003**, *13*, 73–79.

(6) Shalom, M.; Ruĥle, S.; Hod, I.; Yahav, S.; Zaban, A. *J. Am. Chem. Soc.* **2009**, *131*, 9876–9877.

(7) Anikeeva, P. O.; Madigan, C. F.; Halpert, J. E.; Bawendi, M. G.; Bulovic, V. *Phys. Rev. B: Condens. Matter* **2008**, *78*, 085434.

(8) Vossmeyer, T.; Katsikas, L.; Giersig, M.; Popovic, I. G.; Diesner, K.; Chemseddine, A.; Eychmueller, A.; Weller, H. *J. Phys. Chem.* **1994**, *98*, 7665–7673.

(9) Murray, C. B.; Norris, D. J.; Bawendi, M. G. *J. Am. Chem. Soc.* **1993**, *115*, 8706–8715.

(10) Ekimov, A. I.; Hache, F.; Schanne-Klein, M. C.; Ricard, D.; Flytzanis, C.; Kudryavtsev, I. A.; Yazeva, T. V.; Rodina, A. V.; Efros, A. L. *J. Opt. Soc. Am. B* **1993**, *10*, 100–107.

(11) Cumberland, S. L.; Hanif, K. M.; Javier, A.; Khitrov, G. A.; Strouse, G. F.; Woessner, S. M.; Yun, C. S. *Chem. Mater.* **2002**, *14*, 1576–1584.

(12) Arl, D.; Dalmasso, S.; Bozzolo, N.; Zhang, Y.; Gaumet, J.-J.; Laurenti, J.-P. *Mater. Chem. Phys.* **2010**, in press.

(13) Dance, I. G.; Choy, A.; Scudder, M. L. *J. Am. Chem. Soc.* **1984**, *106*, 6285–6295.

(14) Angelova, D.; Armelao, L.; Gross, S.; Kickelbick, G.; Seraglia, R.; Tondello, E.; Trimmel, G.; Venzo, A. *Appl. Surf. Sci.* **2004**, *226*, 144–148.

(15) Sorensen, L.; Strouse, G. F.; Stiegman, A. E. *Adv. Mater.* **2006**, *18*, 1965–1967.

(16) Gacoin, T.; Lahlil, K.; Larregaray, P.; Boilot, J.-P. *J. Phys. Chem. B* **2001**, *105*, 10228–10235.

(17) Reisfeld, R. *J. Alloys Compd.* **2002**, *341*, 56–61.

(18) Green, O. B. *Chem. Commun.* **1999**, *22*, 2235–2241.

(19) Gaumet, J.-J.; Khitrov, G. A.; Strouse, G. F. *Nano Lett.* **2002**, *2*, 375–379.

(20) Gaumet, J. J.; Strouse, G. *Mater. Sci. Eng.: C* **2002**, *19*, 299–304.

(21) Lover, T.; Henderson, W.; Bowmaker, G. A.; Seakins, J. M.; Cooney, R. P. *Inorg. Chem.* **1997**, *36*, 3711–3723.

(22) Magnand, C. *Traité de microscopie électronique*; Hermann: Paris, 1961.

(23) Arl, D.; Aubriet, F.; Gaumet, J.-J. *J. Mass Spectrom.* **2009**, *44*, 763–771.

(24) Khitrov, G. A.; Strouse, G. F. *J. Am. Chem. Soc.* **2003**, *125*, 10465–10469.

(25) Inoue, H.; Ichiroku, N.; Torimoto, T.; Sakata, T.; Mori, H.; Yoneyama, H. *Langmuir* **1994**, *10*, 4517–4522.

(26) CRC *Handbook of chemistry and physics*,83th ed.; CRC Press: Cleveland, 2002.

(27) Wang, Y.; Herron, N. *Phys. Rev. B* **1990**, *42*, 7253–7255.

(28) Spanhel, L.; Haase, M.; Weller, H.; Henglein, A. *J. Am. Chem. Soc.* **1987**, *109*, 5649–5655.

(29) Liu, B.; Xu, G. Q.; Gan, L. M.; Chew, C. H.; Li, W. S.; Shen, Z. X. *J. Appl. Phys.* **2001**, *89*, 1059–1063.

(30) Pradhan, N.; Efrima, S. *J. Am. Chem. Soc.* **2003**, *125*, 2050–2051.

(31) Chrysochoos, J. *J. Phys. Chem.* **1992**, *96*, 2868–2873.

(32) Vuylsteke, A. A.; Sihvonen, Y. T. *Phys. Rev.* **1959**, *113*, 40 LP - 42.

(33) Cao, H.; Wang, G.; Zhang, S.; Zhang, X.; Rabinovich, D. *Inorg. Chem.* **2006**, *45*, 5103–5108.

(34) Peng, X.; Wickham, J.; Alivisatos, A. P. *J. Am. Chem. Soc.* **1998**, *120*, 5343–5344.

(35) Yu, W. W.; Qu, L.; Guo, W.; Peng, X. *Chem. Mater.* **2003**, *15*, 2854–2860.

JP104233X